Evolution of Chaos in the Matsumoto-Chua Circuit: a Symbolic Dynamics Approach

Dariel M. Maranhão and Carmen P. C. Prado
Instituto de Física, Universidade de São Paulo
Caixa Postal 66318, 053015-970, São Paulo, SP, Brazil

Received on 21 July, 2004

We use symbolic dynamics to follow the evolution of the Matsumoto-Chua circuit in the chaotic regime. We consider the evolution of the whole population of unstable periodic orbits and of the associated trajectories, in four chaotic attractors generated by the circuit. Symbolic planes and first return maps are built for different values of the control parameter. The bifurcation mechanism suggests the possibility of the existence of a homoclinic orbit.

1 Introduction

We use symbolic dynamics to revisit the well-studied Matsumoto-Chua circuit. In this analysis we follow the behavior of the whole population of unstable periodic orbits and of the associated trajectories, in four chaotic attractors generated by Chua's circuit in the chaotic regime. With a convenient embedding, we use a natural partition that seems to elucidate the specific bifurcation mechanism characterizing the evolution of the chaotic regime in the system, for a certain range of the control parameter. We show that there is a pattern in the way new (unstable) periodic orbits are created, which is very similar to the mechanism that leads to a homoclinic orbit in one-dimensional systems. The analysis of the symbolic sequences of the trajectories of the circuit, through its fragmentation patterns [6], reinforces the conjecture that the model may present a homoclinic orbit.

This work is organized as follows. In section 2, we present the Matsumoto-Chua circuit as well as the spiral-like attractors associated with this model for a range of values of the control parameter R. In section 3, we identify and extract the unstable periodic orbits and present the partitions used to codify orbits and trajectories. We discuss the hyperbolic regime and show that the evolution of this circuit is very similar to one-dimensional systems with homoclinic chaos. In section 4, we show how the changes in the dynamics of the circuit affects first return maps, symbolic planes and fragmentation patterns. Finally, in section 5, we summarize our conclusions.

2 The Matsumoto-Chua circuit

The Matsumoto-Chua circuit is a simple electronic circuit made of two capacitors, one linear resistor, one inductor, and one nonlinear diode (see Figs. 1(a) and 1(b)). This circuit is modeled by the equations

$$\begin{aligned} C_1\frac{dv_1}{dt} &= \frac{(v_2-v_1)}{R} - h(v_1)\,, \\ C_2\frac{dv_2}{dt} &= \frac{(v_1-v_2)}{R} + i_L\,, \\ L\frac{di_L}{dt} &= -v_2\,, \end{aligned} \tag{1}$$

where C_1 and C_2 are the capacitors, v_1 and v_2 the tensions across the capacitors C_1 and C_2, R is the linear resistor, L is the inductor, i_L is the current across the inductor L, and $h(v_1)$ is the characteristic curve in the (nonlinear) diode. The function $h(v_1)$ (see Fig. 1(b)) is given by

$$h(v_1) = m_1 v_1 + \frac{1}{2}(m_2 - m_1)(|v_1 + B_P| - |v_1 - B_P|)\,, \tag{2}$$

where m_1, m_2, and B_P are constants. We fixed the following values for these parameters: $1/C_1 = 9.0$, $1/C_2 = 1.0$, $1/L = 7.0$, $m_1 = -0.5$, $m_2 = -0.8$ and $B_P = 1.0$; R the control parameter of the model.

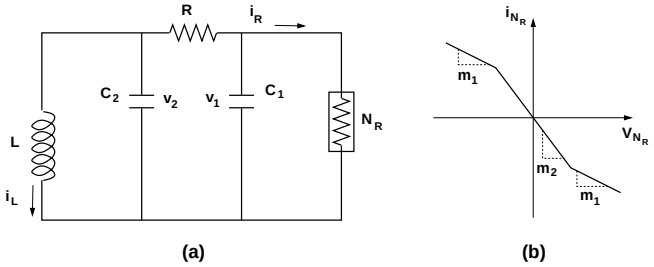

Figure 1. (a)Chua's circuit, with two capacitors (C_1 and C_2), one linear resistor (R), one linear inductor (L), and a nonlinear diode (N_r). (b) Characteristic curve of the non-linear diode.

As the parameter R changes, the Matsumoto-Chua circuit exhibits a complex and rich behavior. This richness has

been explored extensively in previous works (see for example [8]). For $R \approx 1.55$, we can identify a symmetric pair of spiral-like attractors that, after a frontier crisis that occurs for $R \approx 1.47$, merge into a single attractor called by us "double-scroll". In this work we analyze in detail the pair of spiral-like attractors for $R = 1.510$, $R = 1.500$, and $R = 1.495$, which we call A, B, and C, respectively. Because the pair of attractors is symmetric, only one of them needed to be analyzed. The results for attractors A, B, and C, are then compared with results obtained for a forth attractor, D, that appears for a slightly larger value of $R = 1.488$, right after what may be the the onset of a hyperbolic regime.

All the attractors were obtained from numerical integration of equations 1. As an example, a picture of attractor B can be seen in figure 2(a), together with its first return map (fig. 2(b)). Attractors A, B and C show a similar behavior. Attractor D will be better discussed in section 4.

In order to build the first return maps, we used a Poincaré section $P_{v_1^+}$ defined by

$$P_{v_1^+} = \left\{ (v_1, v_2, i_L) \in R^3 \mid v_1 = v_1^+ = \frac{m_2 - m_1}{1/R + m_1},\ v_2 < v_2^+ = 0 \right\}, \tag{3}$$

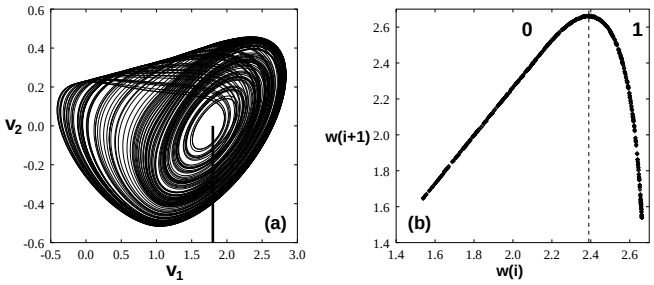

Figure 2. (a) Spiral-like attractor B, ($R = 1.500$), obtained from numerical integration of eq. (1). The full vertical line indicates the Poincaré section $P_{v_1^+}$ from which the first return map (b) was obtained. Attractors A and C present a similar behavior.

where $(v_1^+ = \dfrac{m_2 - m_1}{1/R + m_1}, v_2^+ = 0, i_L^+ = -v_1^+)$ define one of the fixed points of the attractor. Following [9], and taking advantage of the equivariant symmetry presented by the model, we adopted, for the first return map, a new variable $w = |i_L| + \epsilon|v_2|$, where ϵ is an empirical factor ($\epsilon = 1.3$ for attractors A, B, C, and 1.2 for attractor D). If the first return map is written in terms of either i_L or v_2, the branches are shown in duplicate, which makes it more difficult to identify the critical points and, consequently, establish the correct partition needed to code the dynamics. In Fig. 2(b) we see that, for attractor B, the first return map has two branches and a single critical point (at $w = w_c$), as an unimodal map. As usual, we associate the symbol **0** with the left branch ($w < w_c$) and the symbol **1** with the right branch ($w > w_c$). We observe essentially the same scenario for attractors A and C. However, that does not happen for attractor D (see Fig. 4(d)). Now the first return map is bimodal, and we will need three symbols to code the dynamics.

3 Unstable periodic orbits and symbolic dynamics

We combined two numerical methods to extract the unstable periodic orbits from attractors A, B, C and D [9]. First, we estimate the positions of the unstable periodic orbits with a method known as close returns [10]. We then refined the estimate employing a Newton-Raphson algorithm, adapted to differential equations [11]. Each periodic orbit can then be identified by a (finite) sequence of points $w(i)$, that are the intersections of the orbit with a Poincaré section (in our case defined by (3)). The sequence of points $w(i)$ is then codified into a symbolic sequence S_i of zeros and ones, following the usual procedure [7, 4, 5]. The results of applying this procedure to attractors A, B and C are shown in tables I, II and III, respectively. In the tables, for each orbit, one can see the coordinates i_L and v_2 of the intersections of the orbit with the Poincaré section $P_{v_1^+}$, its period, and the symbolic sequence that represents it.

TABLE I. Spectrum of unstable periodic orbits for attractor A up to period 4. For each orbit the table shows the period, the total number of orbits with the same period, coordinates v_2 and i_L, orbital period and symbolic sequence. Coordinates v_2 an i_L are the coordinates of the (negative) periodic point farthest in the Poincaré section $P_{v_1^+}$. The orbit codified by the symbol **0** is pruned and does not appear in the attractor.

period	orbits found	v_2	i_L	orbital period	symbolic sequence
1	1	0.375245	2.110601	3.258975	1
2	1	0.400512	2.149006	6.432970	10
3	2	0.401600	2.164640	9.644468	101
		0.409619	2.171327	9.569009	100
4	3	0.398906	2.158945	12.923580	1011
		0.411168	2.182921	12.738679	1001
		0.414299	2.183881	12.694483	**1000**

TABLE II. Spectrum of unstable periodic orbits for attractor B up to period 6. For each orbit the table shows the period, the total number of orbits with the same period, coordinates v_2 and i_L, orbital period and symbolic sequence. Coordinates v_2 an i_L are the coordinates of the (negative) periodic point farthest in the Poincaré section $P_{v_1^+}$. The orbit codified by the symbol **0** is pruned and does not appear in the attractor.

period	orbits found	v_2	i_L	orbital period	symbolic sequence
1	1	0.355969	2.060343	3.279190	1
2	1	0.380220	2.098244	6.461487	10
3	2	0.380330	2.112240	9.696066	101
		0.388819	2.119516	9.603776	100
4	3	0.378275	2.107688	12.992824	1011
		0.388977	2.129868	12.804077	1001
		0.393345	2.131243	12.734498	1000
5	6	0.379110	2.109425	16.264183	10111
		0.383923	2.107424	16.170103	10110
		0.387477	2.126501	16.109447	10011
		0.389686	2.122016	16.062037	10010
		0.393488	2.138606	15.911679	10001
		0.395959	2.138435	15.866200	10000
6	9	0.378759	2.108697	19.546526	101111
		0.382473	2.103817	19.459271	101110
		0.385952	2.123788	19.283093	100101
		0.388119	2.127780	19.375027	100111
		0.391105	2.125702	19.309144	100110
		0.392440	2.136122	19.220406	100011
		0.394071	2.133682	19.189325	100010
		0.396380	2.143670	19.036973	100001
		0.397506	2.143324	19.018181	**100000**

TABLE III. Spectrum of unstable periodic orbits for attractor C up to period 7. For each orbit the table shows the period, the total number of orbits with the same period, coordinates v_2 and i_L, orbital period and symbolic sequence. Coordinates v_2 an i_L are the coordinates of the (negative) periodic point farthest in the Poincaré section $P_{v_1^+}$. The orbit codified by the symbol **0** is pruned and does not appear in the attractor.

period	orbits found	v_2	i_L	orbital period	symbolic sequence
1	1	0.346631	2.035522	3.289718	1
2	1	0.370350	2.073135	6.476573	10
3	2	0.370110	2.086434	9.722736	101
		0.378688	2.093893	9.622686	100
4	3	0.368286	2.082318	13.029050	1011
		0.378391	2.103745	12.837062	1001
		0.383089	2.105259	12.758032	1000
5	6	0.369006	2.083846	16.311586	10111
		0.373797	2.081734	16.210760	10110
		0.377097	2.100762	16.150964	10011
		0.379468	2.096118	16.096295	10010
		0.382666	2.112373	15.954404	10001
		0.385671	2.112181	15.897681	10000
6	9	0.368712	2.083222	19.604144	101111
		0.372478	2.078432	19.510288	101110
		0.375699	2.098180	19.328885	100101
		0.377634	2.101866	19.428620	100111
		0.380821	2.099620	19.353596	100110
		0.381782	2.110216	19.269788	100011
		0.383745	2.107347	19.229038	100010
		0.385310	2.117473	19.098146	100001
		0.387337	2.116889	19.067501	100000

Continuation.

period	orbits found	v_2	i_L	orbital period	symbolic sequence
7	18	0.368828	2.083468	22.892743	1011111
		0.370050	2.086053	22.753241	1011011
		0.373016	2.079778	22.795416	1011110
		0.373846	2.081856	22.685489	1011010
		0.376020	2.098544	22.633431	1001011
		0.377418	2.101425	22.722940	1001111
		0.378068	2.103082	22.559760	1001101
		0.379304	2.095697	22.573458	1001010
		0.380283	2.098224	22.653816	1001110
		0.380954	2.108957	22.444587	1000101
		0.381248	2.100457	22.471575	1001100
		0.382171	2.110981	22.544866	1000111
		0.383375	2.106013	22.380280	1000100
		0.384411	2.109156	22.489943	1000110
		0.384689	2.115781	22.403247	1000011
		0.386120	2.113963	22.373126	1000010
		0.387501	2.121359	22.350529	1000001
		0.388674	2.121168	22.377672	**1000000**

The dynamics of the system, in cases where it can be coded by two symbols only (unimodal maps), can be represented by a diagram known as the alternating binary tree (see Fig. 3). The alternating binary tree represents all sequences that form the itinerary; they appear in a specific order, known as "natural order" [11]. A given orbit is represented by the specific sequence - among all compatibles with its itinerary - that appears most at right in the alternating binary tree. It can be proved that, for unimodal maps [12], if an specific orbit is present in a dynamical system, all the other orbits that precede it according to the natural order will also be present. An inspection of Fig. 3 shows that, periodic orbits of period n, represented by sequences of the form $s_h^{(n)} = \underbrace{(100...0)}_{n}$ (one followed by $(n-1)$ zeros) are always at the extreme right of the binary tree. So, the identification of an orbit of the type $s_h^{(n)}$ means that the system has all possible orbits, up to level n.

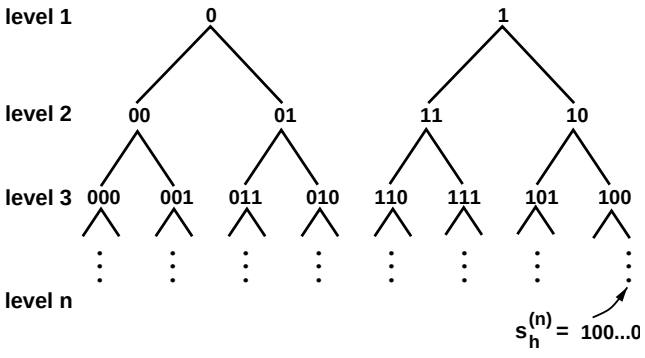

Figure 3. Alternating binary tree for unimodal maps. In this diagram the periodic orbits are ordered in a natural sequence, from left to right. If a periodic orbit is present in the attractor, all other orbits that precede it in this tree are also present.

An orbit predicted by the alternating binary tree, but not found in the dynamical system, is said to have been "pruned". Note that, in the case of attractor A, some orbits start to be pruned for $n = 5$ (see table I). The same behavior can be observed in attractors B and C. But in those cases orbits start to be pruned for $n = 7$, and $n = 8$, respectively (see tables II and III). Note that the period 1 orbit represented by the symbolic sequence **0** is not present in any of the attractors.

In one-dimensional maps, as a dynamical system approaches homoclinicity, that is, as the unstable manifold W^u, associated with a saddle cycle or a saddle point approaches and touches a stable manifold W^s, many homoclinic points are created. As a consequence, the dynamics of the system becomes more and more complex, with more and more unstable periodic orbits. After the last tangency between manifolds W^u and W^s, there is an infinite number of homoclinic points. When the homoclinic orbit appears, the dynamics reaches its highest degree of complexity; all possible periodic orbits are present and the alternating binary tree is complete. We then say that the system has reached the hyperbolic regime.

A homoclinic orbit can be represented by the symbolic sequence $\mathcal{O}_H = 1000... = s_h^{n\to\infty} = (100...)$ [2]. The symbol "**1**" represents the re-injection of the orbit towards the saddle cycle, while the infinite number of symbols "**0**" represent the divergent movement of the orbit around this point. Such an orbit is represented by the last sequence that appears in a complete and infinite alternating binary tree, so the observation of a homoclinic orbit in a dynamical system implies the existence of an infinite number of unstable periodic orbits, of all possible periods. The occurrence of a homoclinic orbit has been identified as the mechanism responsible for the onset of chaos in many dynamical systems. The Rossler attractor [1] and some experimental systems as glow discharge [2] or lasers with a saturable absorber [3] are well-studied examples of more complex systems that have

their chaotic behavior associated with the presence of a homoclinic orbit. In such cases the system is said to display homoclinic chaos. The analysis of those dynamical systems has been based on the identification of homoclinic bifurcations [3] - a sequence of saddle-node bifurcations that alternates with period-doubling bifurcations - that leads to the appearance of a homoclinic orbit. The occurrence of such a sequence of bifurcations, before the observation of a homoclinic orbit, has many times been considered sufficient to assume homoclinicity. This sequence induces a ramified structure in first-return maps, builded in a special way so they can capture the number of turns that a trajectory performs around a saddle point (or an unstable hyperbolic saddle cycle [2, 3]) before being reinjected in the attractor. Each of the branches of the first-return maps is associated with a specific number of turns that the system gives around the unstable saddle point or cycle.

The extrapolation, for smaller values of the control parameter R, of the sequence of unstable periodic orbits found in attractors A, B and C (and shown, respectively, in tables I, II and III), allows us to conjecture about the existence of a homoclinic orbit $\mathcal{O}_{\mathcal{H}}$. This is better seen in table IV, which shows, for attractors A, B and C, the last level n for which all sequences predicted by the alternating binary tree have been found. One can observe that the last sequence in the alternating binary tree is, up to some level n, of the form $s_h^{(n)} = \underbrace{(100...0)}_{n}$, with increasing values of n for decreasing values of R. The increase in the number of zeros in the orbits of table IV is associated with an increase in the divergent movement around the saddle cycle, in a typical behavior of systems with a homoclinic orbit. This observation gives support to a conjecture that, in the Matsumoto-Chua circuit, as the parameter R decreases, new orbits of period n $s_h^{(n)} = (100...0)$ are created, filling up every level of the binary tree until the hyperbolic regime is attained. The analysis of the symbolic planes and fragmentation patterns gives further support to this conjecture.

TABLE IV. Last level (and the corresponding symbolic sequence) that presents a complete spectrum of orbits in the alternating binary tree, for attractors A, B and C.

attractor	R	level n	$s_h^{(n)}$
A	1.510	4	(1000)
B	1.500	6	(100000)
C	1.495	7	(1000000)

4 Symbolic planes

The changes in the dynamics introduced by the development of chaos in the Matsumoto-Chua circuit can be observed both in the first-return maps and in the symbolic planes, for attractors A, B, C, and D.

The symbolic plane gives a way of summarizing the ordering of symbolic sequences in a two-dimensional map. This method has been widely employed to identify topologically similar systems (see examples in references [13], [15] and [14]). Each point (α, β) in a Cartesian plane is associated with a possible sequence in a way described below. If all possible orbits are present, the plane is completely filled. Empty points, represent orbits that have been pruned and are forbidden. From the symbolic plane it is possible to identify the pruning fronts and the kneading sequences.

The coordinates (α, β) of a specific orbit or trajectory is built in a unique way from the symbolic sequence of zeros and ones that represents the orbit, through the following procedure. Let the symbolic sequence

$$\ldots s_{-m} \ldots s_{-2} s_{-1} s_0 s_1 s_2 \ldots s_m \ldots \qquad s_i \in 0, 1 \,, \tag{4}$$

represent a given trajectory. The symbol s_0 (representing the current position of the system) splits the sequence into two parts, a forward sequence given by $s_0 s_1 s_2 \ldots s_m \ldots$ which represents the "symbolic future", and a backward sequence $\ldots s_{-m} \ldots s_{-2} s_{-1}$, which represents the "symbolic past". The symbolic coordinates (α, β) for the point that will represent this orbit are then given, in binary notation, by

$$\alpha = 0.a_1 a_2 a_3 \ldots \,, \qquad \beta = 0.b_1 b_2 b_3 \ldots \,, \tag{5}$$

where

$$a_i = \sum_{j=0}^{i-1} s_j \;\; (mod 2) \,, \qquad \text{and} \qquad b_i = \sum_{j=1}^{i} s_{-j} \;\; (mod 2) \,, \tag{6}$$

where α and β correspond to real numbers, given by

$$\alpha = \sum_{i=1}^{m} \frac{a_i}{2^i}, \qquad \beta = \sum_{i=1}^{m} \frac{b_i}{2^i} \,. \tag{7}$$

This formalism can be extended to represent a dynamics described by 3 or more symbols (see, for example,[15] and [16]).

In Figs. 4(a), 4(b), 4(c) and 4(d) we can see the first return maps and the symbolic planes for attractors A, B, C and D, respectively. The first return maps of attractors A, B and C show that those attractors have a unimodal behavior, and can essentially be described by a symbolic dynamics made of two symbols. The first-return map for attractor A ($R = 1.510$) indicates that the system does not have all possible orbits; the symbolic plane shows many forbidden regions (empty regions) together with allowed regions (filled with dots). Comparing with Figs. 4(b) and 4(c) (attractors B and C, for $R = 1.500$ and $R = 1.495$, respectively) we notice that the left branch of the first-return map approaches more and more the diagonal, and less orbits are forbidden. Fig. 4(c) captures the dynamics in a point with almost no forbidden orbits.

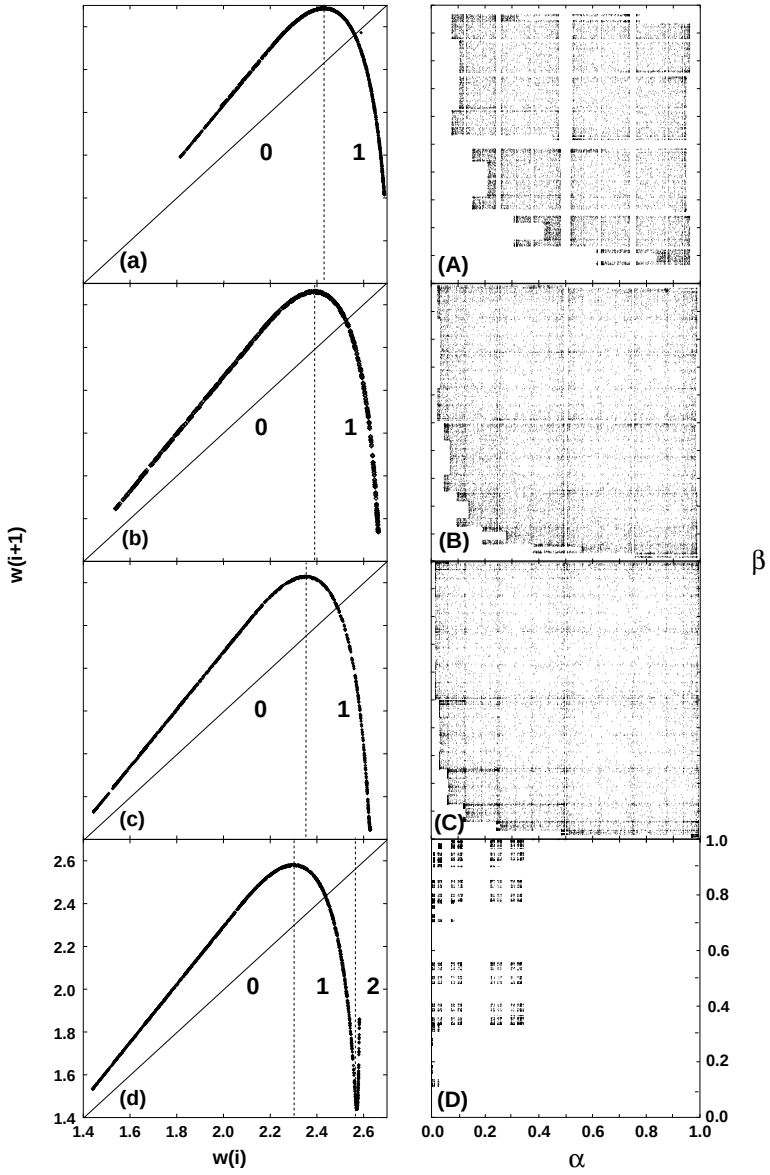

Figure 4. First-return maps and corresponding symbolic planes for attractors A,B, C and D respectively. We can observe that, as the parameter R decreases, the symbolic plane is more and more complete. From A to C the symbolic planes show an increase in the allowed regions, indicating the approach of the hyperbolic regime. Attractor D shows a complete different scenario. The first-return map is not unimodal anymore, and in the symbolic plane (now associated with a symbolic dynamics of three symbols) we observe a predominance of forbidden regions.

Figure 4(d) (attractor D, with $R = 1.488$) shows a completely different scenario, with the drastic changes in the behavior of the system that may have been induced by the onset of a homoclinic regime. Now the first-return map is bimodal. The symbolic plane, now built with a dynamics of three symbols, is completely different, with many forbidden regions.

In unimodal maps with a unidimensional structure, the pruning front, in the symbolic plane, is a continuous line, while in two-dimensional maps the pruning front is discontinuous [14]. Fig. 5, an amplification of the symbolic planes presented in Fig. 4, clearly shows that there is a discontinuity in the pruning fronts of attractors A, B and C, indicating that they do have a two-dimensional structure. We see, however, that those pruning fronts get closer and closer to each other as we go from attractor A to C [1]. In order to measure how good is the one-dimensional approximation, we can define an index d, equal to the integer part of $\log_2(\frac{1}{\alpha_2 - \alpha_1})$, where α_1 and α_2 define the smaller and larger pruning fronts, respectively. The index d gives the level, in the binary tree, up to which the behavior of the system can be considered one-dimensional. For instance, for attractor A, $\alpha_1 = 0.9472$ and $\alpha_2 = 0.9605$, so $d_A = 4$. Analogously, $d_B = 7$ and $d_C = 11$. Those results show that the one-dimensional approximation becomes better and better as the chaotic regime evolves.

[1] notice that, in order to show the existence of a discontinuity, the scales of each symbolic plane of Fig. 5 are not the same.

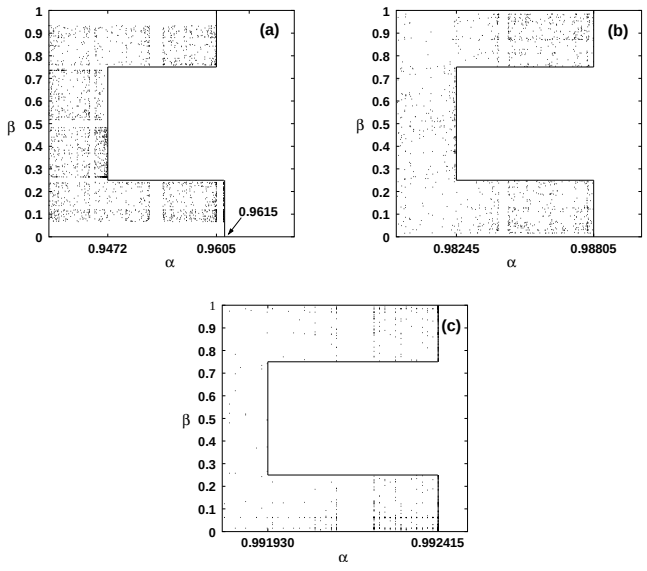

Figure 5. Blow up of the pruning front region of Figs. 4A, 4B and 4C, showing the two-dimensional structure of attractors A, B and C.

We are aware that, if we have a 2D map, the existence of a 10^n orbit does not force the existence of all previous orbits of the natural sequence, as it happens in 1D maps. However, we think that we have strong indications that, at least in these case, as the chaotic regime evolves and the dynamics of the system becomes more and more one-dimensional, it approaches the dynamical behavior of a typical unimodal map, and our observations may in fact indicate the existence of homoclinic chaos. It would be interesting to observe if, in other systems, for which it is well established that the hyperbolic regime is reached, the same scenario is found.

The fragmentation patterns (see Fig. 6) give another way of showing that Chua's circuit may be approaching a homoclinic regime. Through those patterns one can build a pictorial representations of the symbolic sequences that represent the trajectories. We associate a black block with symbol **1** and a white block with symbol **0**. For instance, the sequence **100** would be represented by the sequence of blocks "black-white-white". The blocks are placed in sequence, side by side, from left to right, up to 50 blocks; after that, a new row of symbols is added on top of the previous one. The process continues until a grid of 50×50 blocks is built. As the chaotic regime evolves, the allowed trajectories will present an increasing number of symbols **0**, associated with the divergent movement around the saddle cycle, as compared to the number of symbols **"1"**, associated with the reinjection movement.

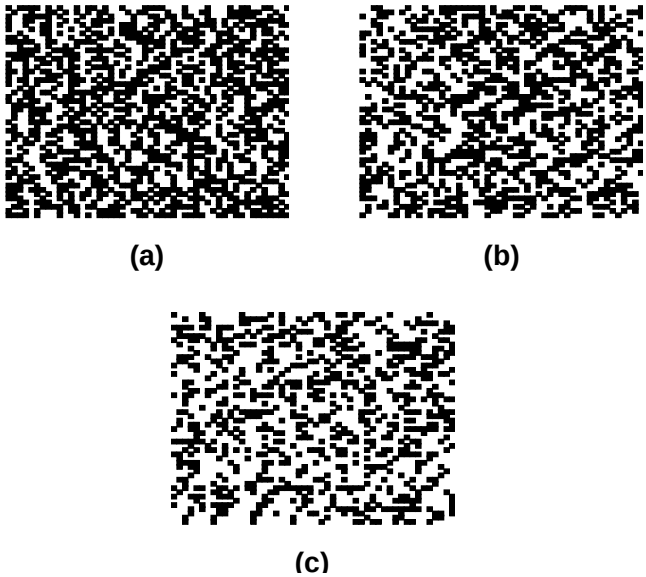

Figure 6. Fragmentation patterns for symbolic sequences of attractors A, B and C respectively.

By visual inspection, it is possible to see that the orbits of attractor A (Fig. 6a) have a predominance of symbols **1** (black blocks), while in attractor C (Fig. 6c) there is a predominance of symbols **0**, reflecting the fact that, as the parameter R decreases, the trajectories stay longer and longer in a divergent movement around the saddle cycle.

5 Conclusions

In conclusion, we have extracted the unstable periodic orbits from attractors A, B, C and D of the Matsumoto-Chua circuit. We have used symbolic dynamics in order to show that as the chaotic regime evolves the Matsumoto-Chua circuit has a dynamics that is increasing one-dimensional. We have presented numerical evidence that a homoclinic orbit may be present in the Matsumoto-Chua circuit. The attractors of the dynamics of the circuit were analyzed for four different values of the control parameter R, $R \in [1.510, 1.4888]$. We found that there is a pattern in the way new unstable periodic orbits are created as the control parameter R is continuously decreased. From this pattern, if the system had a truly 1D dynamics, it would be possible to infer the existence of a homoclinic orbit. If this behavior comes to be checked in similar systems, it will be a new approach to the problem of identifying the onset of homoclinicity that could be used in many other problems, either in experimental situations or numerical simulations.

For each of the studied attractors (attractors A, B and C), we have extracted the unstable periodic orbits, built first-return maps, codified the dynamics and ordered the orbits according to the natural order in an alternating binary tree. It has been possible to see that the last orbit in the diagram, before orbits start to be pruned, was always of the form $s^{(n)} = \underbrace{(100...0)}_{n}$, with $n \to \infty$ as the parameter R decreases. Every level of the binary tree is then filled up

as in a one-dimensional map, until the hyperbolic regime is attained. We conjecture that, because the behavior of the system becomes close to a one-dimensional map, maybe a homoclinic orbit exists in this circuit.

We also built symbolic planes and fragmentation patterns for all the studied sequences and trajectories, which gives further support to our conjecture.

6 Acknowledgements

We acknowledge the financial support of the Brazilian agency CNPq.

References

[1] P. Gaspard, R. Kapral, G. Nicolis, J. Stat. Phys. **35**, 697 (1984).

[2] T. Braun, J. A. Lisboa, Int. J. Bifurc. Chaos, **4**, 1483 (1994).

[3] F. Papoff, A. Fioretti, E. Arimondo, Phys. Rev. A **44**, 4639 (1991).

[4] J. Plumecoq, M. Lefranc, Physica D **144**, 231 (2000).

[5] N. B. Tufillaro, T. Abbott, J. Reilly, *An experimental approach to nonlinear dyanamics and chaos* (Addison-Wesley, California, 1992).

[6] W. M. Gonçalves, R. D. Pinto, J. C. Sartorelli, Physica D **134**, 267 (1999).

[7] J. Milnor and W. Thurston, in Dynamical Systems, ed. J. Alexander, Lecture Notes in Math. **1342**, spring-Verlag, Berlin, (1988).

[8] R. N. Madan, *Chua's circuit: a paradigm for chaos*, (World Scientific, Singapore, 1993).

[9] C. Letellier, P. Dutertre, G. Gouesbet, Phys. Rev. E **49**, 3492 (1994).

[10] D. P. Lathrop, E. J. Kostelich, Phys. Rev. A **40**, 4028 (1989); G. B. Mindlin, Gilmore, Physica D **58**, 229 (1992).

[11] B. -L. Hao, *Elementary Symbolic Dynamics and Chaos in Dissipative Systems*, (World Scientific, Singapore, 1984).

[12] P. Glendinning, C. Laing, Phys. Letters A **211**, 155 (1996); S. V. Gonchenko, L. P. Shilnikov and D. V. Turaev, Chaos **6**, 15 (1996); R. L. Devaney, *An introduction to chaotic dynamical systems*, (Addison-Wesley, second ed., Boston 1988).

[13] A. Tufaile, J. C. Sartorelli, Phys. Lett. A **275**, 211 (2000).

[14] P. Civitanović, G. H. Gunaratne and I. Procaccia, Phys. Rev. A **38**, 1503 (1988).

[15] C. Letellier, G. Gouesbet and N. F. Rulkov, Int. J. Bifurc. Chaos **6**, 2531 (1996).

[16] J.-X. Liu, W. -M. Zheng and B. -L. Hao, Chaos, Solitons and Fractals **7**, 1427 (1996).